Tandem colloidal quantum dot solar cells employing a graded recombination layer

Xihua Wang[1†], Ghada I. Koleilat[1†], Jiang Tang[1], Huan Liu[1,2], Illan J. Kramer[1], Ratan Debnath[1], Lukasz Brzozowski[1], D. Aaron R. Barkhouse[1], Larissa Levina[1], Sjoerd Hoogland[1] and Edward H. Sargent[1*]

Tuning of the electronic bandgap in colloidal quantum dots (CQDs) by changing their size enables the spectral response of CQD-based photodetectors[1-5] and photovoltaic[6-12] devices to be tailored. Multi-junction solar cells made from a combination of CQDs of differing sizes and thus bandgaps are a promising means by which to increase the energy harvested from the Sun's broad spectrum. Here, we report the first CQD tandem solar cells using the size-effect tuning of a single CQD material, PbS. We use a graded recombination layer to provide a progression of work functions from the hole-accepting electrode in the bottom cell to the electron-accepting electrode in the top cell, allowing matched electron and hole currents to meet and recombine. Our tandem solar cell has an open-circuit voltage of 1.06 V, equal to the sum of the two constituent single-junction devices, and a solar power conversion efficiency of up to 4.2%.

First reported[13] in 2005, full-spectrum quantum dot solar cells have now achieved solar power conversion efficiencies greater than 5% (ref. 14). The capacity to tune the bandgap of colloidal quantum dots (CQDs) has allowed the realization of optimal-bandgap single-junction solar cells. In principle it also allows tandem and multi-junction cells to be realized, devices that raise the ultimate limit on solar cell performance from 31% to 42% (tandem) and 49% (triple-junction)[6].

In this Letter, we report the construction of an efficient recombination layer that is tailored to the requirements of CQD photovoltaics, and we deploy this new technology to demonstrate the first tandem CQD photovoltaic devices. We current-match and stack two depleted-heterojunction CQD solar cells. We use colloidal quantum dots having exciton peaks at 1.6 eV for the visible junction (front cell) and 1 eV for the infrared junction (back cell) (Fig. 1a,b). These bandgaps are within 5% of optimal for a current-matched solar cell[6].

Depleted-heterojunction CQD photovoltaics[14] use TiO_2 to accept the photoelectrons but block the photoholes that are generated in light-absorbing PbS CQD semiconductor layers (Fig. 1c–e). The n-type TiO_2 produces a built-in field at the junction with the p-type PbS CQD film. Electron–hole pairs generated in the CQD film are separated through the combined action of this depletion region and the type-II heterointerface with TiO_2.

In current-matched series-connected tandem solar cells, the hole current from the front cell and the electron current from the back cell must recombine with high efficiency and minimal loss of electrical potential in a suitably designed intervening layer. In epitaxial compound semiconductor devices this is achieved using tunnel junctions[15–18] and in organic photovoltaics using recombination layers[19–22]. In the tunnel junction, degenerately doped p^{++} and n^{++} materials produce a thin junction in which the valence band on the p-side is energetically aligned with the conduction band on the n-side, and the depletion region is sufficiently thin that carriers can tunnel from one side to the other. CQD solids (or materials of similar bandgap and compatible with CQD processing) that achieve the sequential combination of transparent p^{++} followed by n^{++} doping are not available.

We sought a new strategy that would be compatible with CQDs, and that would enable the realization of a highly effective tandem solar cell. We term this new concept a 'graded recombination layer (GRL)'. We present a practical GRL design using spatial band diagrams to depict a CQD tandem cell at equilibrium (Fig. 1c), and under short-circuit (Fig. 1d) and open-circuit conditions (Fig. 1e).

Photoholes from the valence band of the front cell are required to recombine with photoelectrons from the conduction band of the back cell. They must do so without adding appreciably to the series resistance of the overall device. If the deep-work-function contact associated with the front cell were directly connected to the shallow-work-function electron-acceptor of the back cell, a large energetic barrier would impede the flow of electrons necessary for recombination with the holes from the front cell.

The GRL concept overcomes this problem by using a progression of work functions from the front to the back cell. The concept is implemented using a progression of n-type transparent oxides[23] that are both readily available and CQD-compatible. We progress from deep-work-function n-type MoO_3 through intermediate indium tin oxide (ITO) to shallow-work-function but still heavily doped aluminium-doped zinc-oxide (AZO), the work function of which matches that of the lightly doped TiO_2 acceptor. All these materials are deposited using room-temperature sputtering processes compatible with CQD films.

Ideally, the gradual progression of the GRL would achieve barrier-free conveyance of electrons from the back cell to recombine with the holes extracted from the front cell. In our actual devices, relatively small barriers can be seen in Fig. 1c–e. From calculations (Supplementary Section SI3) and the experiments reported here, we find that these barriers are sufficiently readily overcome to allow the GRL to have a series resistance that is sufficiently low to enable a solar cell operating at 1 sun.

Current matching is also required in an optimized tandem cell; the absorbed photon spectrum should be divided equally between the two junctions to match the currents meeting up in the recombination layer. We first measured the absorbance spectrum of PbS CQD films and obtained their absorption coefficients (Fig. 2a).

[1]Department of Electrical and Computer Engineering, University of Toronto, 10 King's College Road, Toronto, Ontario M5S 3G4, Canada, [2]Department of Electronic Science and Technology, Huazhong University of Science and Technology, Wuhan 430074, P. R. China; [†]These authors contributed equally to this work. *e-mail: ted.sargent@utoronto.ca
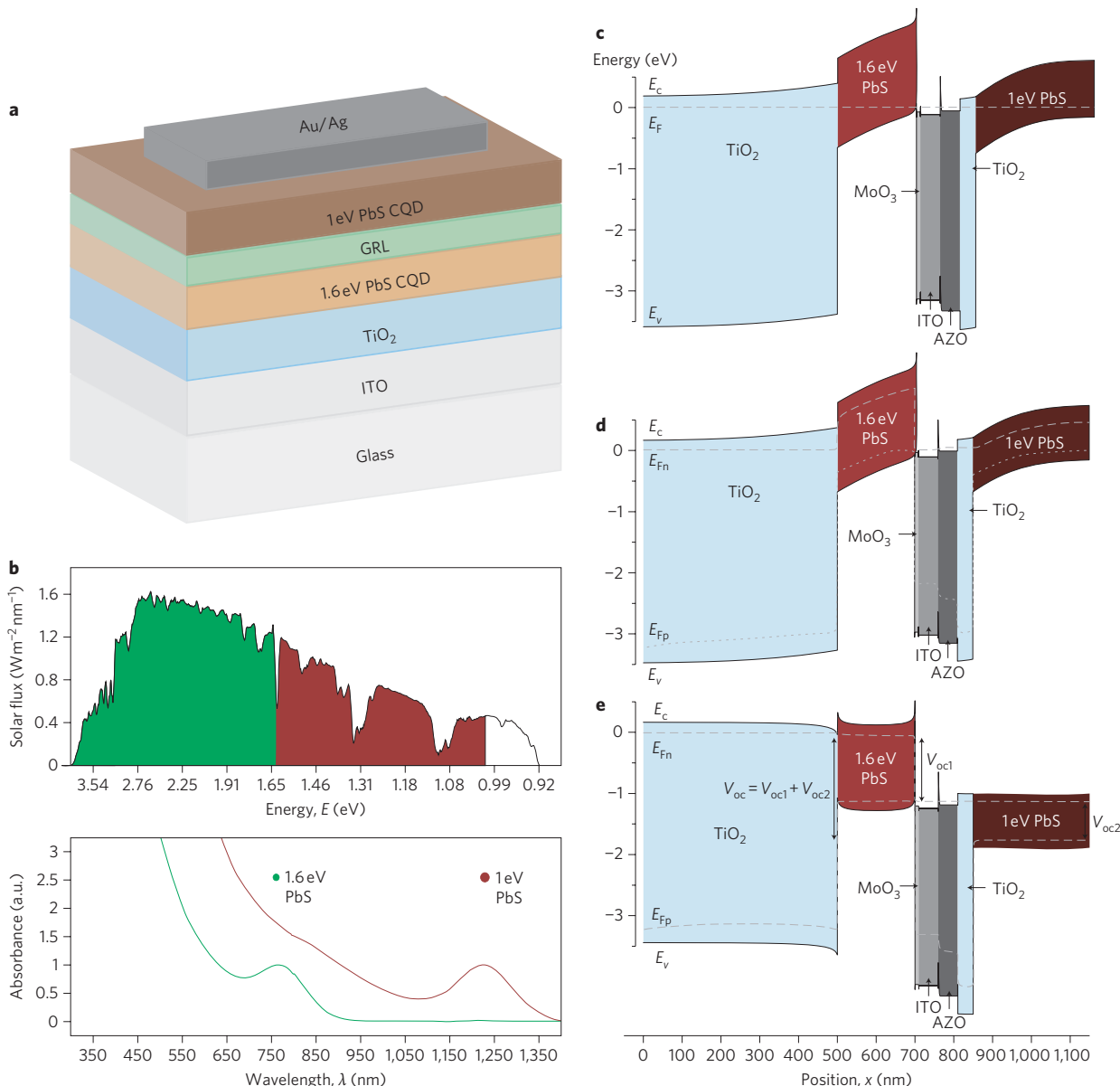
1

Figure 1 | Colloidal quantum dot (CQD) based tandem solar cells: concept and realization. a,b, Device architecture (**a**) and spectral utilization (**b**) for CQD tandem solar cells having quantum-confined bandgaps of 1.6 eV (green) and 1.0 eV (red). **c–e,** Spatial band diagrams for CQD tandem cells at equilibrium (**c**) and under short-circuit (**d**) and open-circuit (**e**) conditions, where E_F is the Fermi energy (dashed-dotted line in **c**), E_{Fn} is the electron quasi-Fermi energy (dashed line in **d** and **e**), and E_{Fp} is the hole quasi-Fermi energy (dotted line in **d** and **e**).

We then determined the total current density from the 200-nm-thick front cell when the internal quantum efficiency (IQE) averaged 70% (Fig. 2b and Supplementary Section SI4). Figure 2b plots the expected current density of the back cell as a function of its thickness when the IQE averages 35% (Supplementary Section SI4). This plot predicts that a back-cell thickness in the range 250–300 nm should achieve current matching.

To verify these calculations, we built a 300-nm-thick infrared-wavelength cell having the usual reflective top contact, and illuminated it through a transparent-top-contact visible-wavelength cell. In this configuration we measured a short-circuit current J_{sc} of 8.7 mA cm^{-2} and 8.9 mA cm^{-2} (Fig. 3a) for the visible and infrared cells. This confirmed that our model had enabled us to achieve current matching to within a few percent.

Figure 3a presents the measured current–voltage characteristics of the constituent junctions and the tandem cell under 100 mW cm^{-2} AM1.5 illumination. Table 1 summarizes the

figures of merit of our devices. The single-junction visible device (with transparent top contact) exhibits an open-circuit voltage V_{oc1} of 0.7 V, J_{sc} of 8.7 mA cm^{-2}, fill factor of 49% and AM1.5 power conversion efficiency (PCE) of 2.98%. The single-junction infrared (IR) device exhibits an open-circuit voltage V_{oc2} of 0.39 V, J_{sc} of 18.6 mA cm^{-2}, fill factor of 42% and AM1.5 PCE of 3.04%. When the visible CQD film is used as a filter, the IR cell J_{sc} drops to 8.9 mA cm^{-2}.

The ideal tandem cell should exhibit a V_{oc} equal to the sum of the open-circuit voltages of the constituent cells. The GRL device achieves an open-circuit voltage of 1.06 V, equal, to within a few percent, to the sum of the open-circuit voltages of the individual single junctions. The tandem CQD photovoltaic device provides an AM1.5 PCE of 4.21%, compared to the ~3% values achieved by its constituents.

The external quantum efficiency (EQE) spectra (Fig. 3b) of the constituent single-junction solar cells further confirm current

matching. The integrated current density of the visible-junction (area under blue curve) was calculated to equal, within 10%, the integrated current density of the IR junction filtered by the visible junction (area under red curve).

As a control, we constructed a tandem device that does not benefit from the GRL. This device directly connected ITO and TiO_2. It exhibited a much lower open-circuit voltage of 0.73 V as well as a weakened short-circuit current compared to the GRL device. We attribute this suboptimal behaviour to the establishment of an undesired barrier to electron flow in the intended cascade from TiO_2 to ITO (Supplementary Section SI3).

We now discuss further the processing and properties of the layers that constitute the GRL. To maintain their performance (for example, low recombination rates) CQD films require a minimum of exposure to reactive oxygen. A layer (10 nm) of MoO_3 was first evaporated onto the CQD films, serving both as the deep-work-function n^{++} layer and as a buffer layer to protect against damage during ensuing layer depositions. We designed the layers constituting the GRL to be as thin as possible to minimize parasitic electrical losses while still ensuring complete coverage of the prior layers. We selected 10 nm, 50 nm, 50 nm and 40 nm for the MoO_3, ITO, AZO and TiO_2 layers, respectively.

A detailed electronic materials characterization (Fig. 4) of MoO_3, AZO and TiO_2 is now presented. Table 2 summarizes the measured electron affinity E_c, work function E_f, ionization energy E_v and

Figure 3 | Photovoltaic device performance for tandem and constituent single-junction cells. a, Current–voltage characteristics under AM1.5 1 sun simulated illumination for the large-bandgap (blue) and small-bandgap (black) cells. *J–V* of the small-bandgap device when the large-bandgap CQD film is used as a filter is also shown (red). The tandem cell *J–V* is shown in green. **b**, EQE spectra of the large-bandgap junction with a transparent top contact (blue), the small-bandgap junction with a reflective top contact (black), and the small-bandgap junction with the large-bandgap CQD film used as filter (red). When the large-bandgap CQD film filters the incoming light, the estimated J_{sc} of the small-bandgap junction is matched to the J_{sc} of the large-bandgap junction.
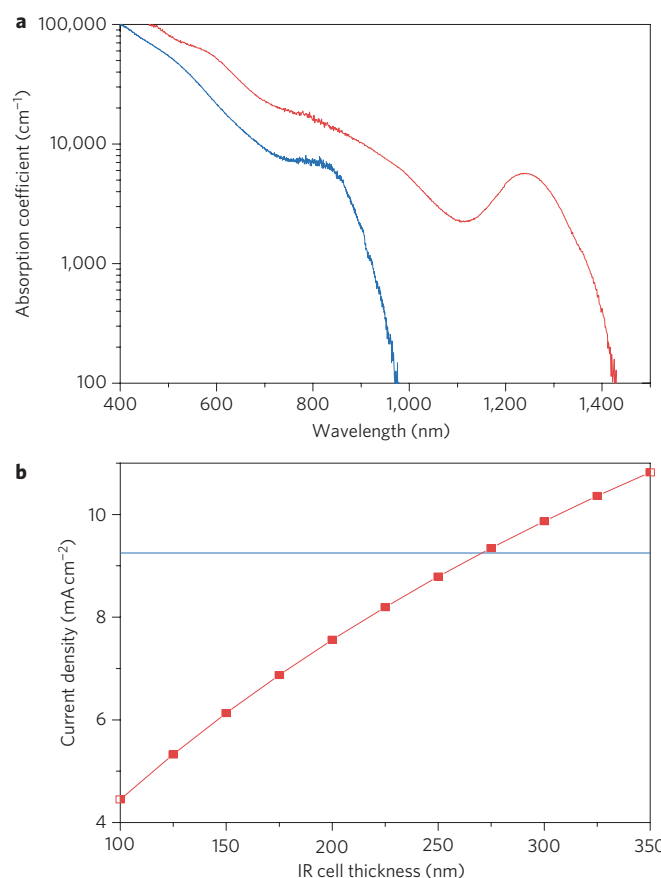
Figure 2 | Design for current matching in CQD tandem cells. a, Measured absorption coefficients of the 1.6 eV bandgap (blue line) and 1.0 eV bandgap (red line) films. **b**, Predicted current densities for the small-bandgap back cell as a function of its thickness. Double-pass absorption due to the reflective top contact is taken into account. Current matching is achieved in the thickness range 250–300 nm. The visible-junction optimal thickness is fixed at 200 nm, generating an expected current density of 9 mA cm^{-2} (blue line).
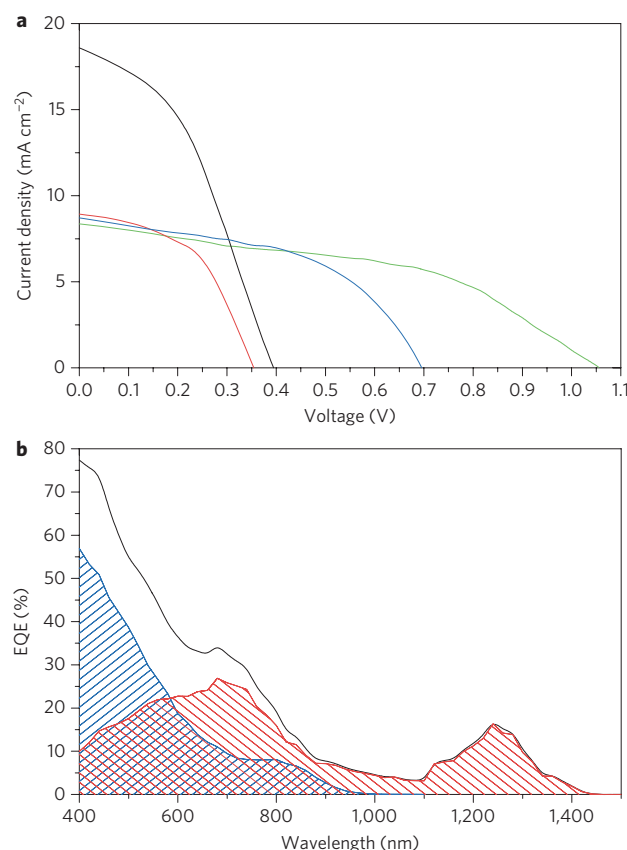
electron free-carrier density n_0 of the metal oxides. Ultraviolet photoelectron spectroscopy (UPS) was used to obtain work functions (SI6). The work functions progress from 5.4 eV (MoO_3) through 4.8 eV (ITO) to 4.1 eV for both AZO and TiO_2. Band edges were also obtained using UPS. For AZO and TiO_2, electron affinities of 4.1 and 4.0 eV, respectively, were measured. We confirmed these values using cyclic voltammetry, which provided the electron affinities directly by means of an alternative measurement.

Field-effect transistor (FET) test structures were constructed to estimate the carrier densities. Doping values of $\sim 1 \times 10^{19}$ and $\sim 5 \times 10^{19}$ cm^{-3} for MoO_3 and AZO, respectively, confirmed that they are heavily doped materials, and the doping value of $\sim 5 \times 10^{16}$ cm^{-3} for TiO_2 confirms its light doping. We found that

Table 1 | Figures of merit of the devices cell under 100 mW cm^{-2} AM1.5 illumination.

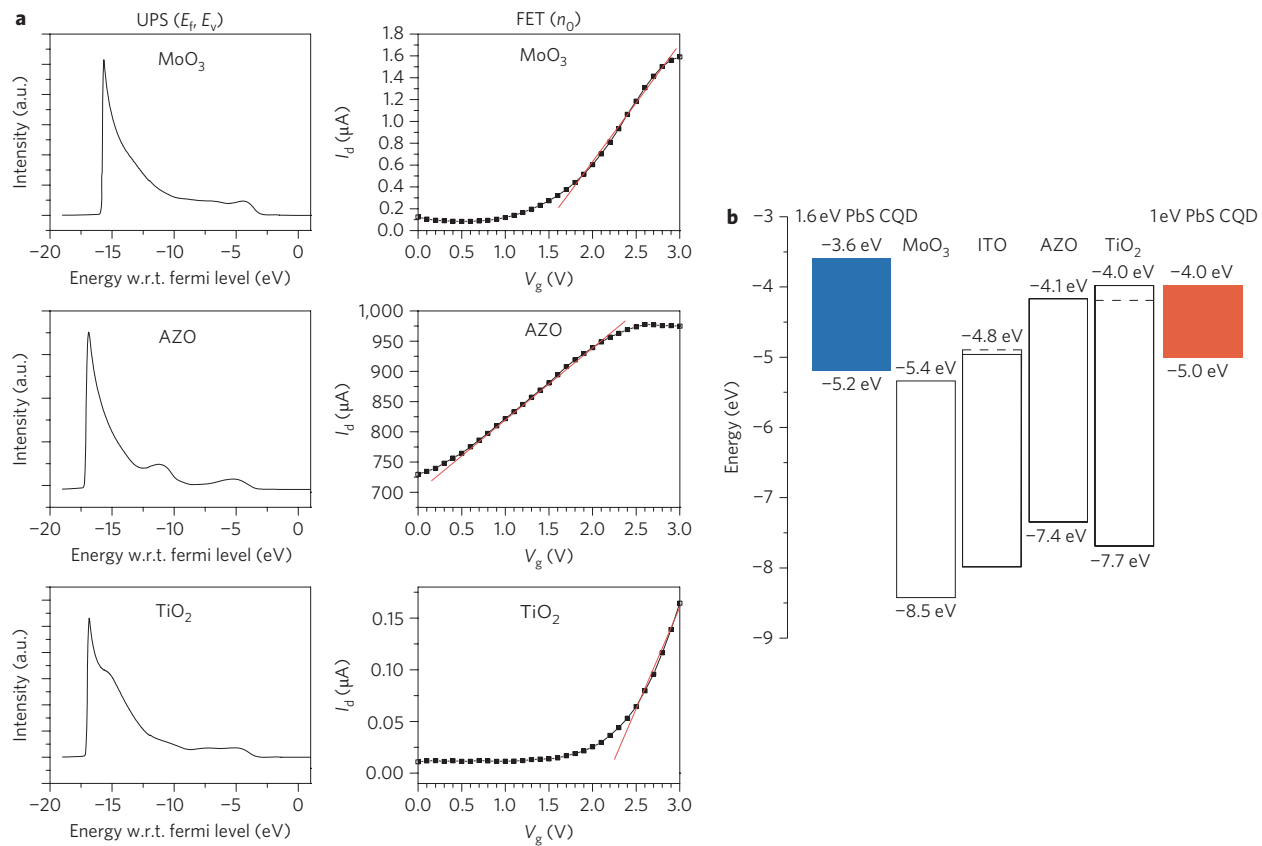| Junctions	J_{sc} (mA cm^{-2})	V_{oc} (V)	FF (%)	PCE (%)
Visible	8.7	0.7	49	2.98
IR	18.6	0.39	42	3.04
IR$_{w/Visible\ filter}$	8.9	0.36	46	1.47
Tandem	8.3	1.06	48	4.21

Figure 4 | Electrical characterization of GRL materials. a, UPS data for MoO_3, AZO and TiO_2 and FET transconductance for MoO_3, AZO and TiO_2.
b, Energy level diagram showing the HOMO and LUMO energies of each type of PbS quantum dot, and the Fermi levels (dashed lines) and band edges of the isolated GRL materials. .

conduction band-edge values obtained from cyclic voltammetry varied by ± 50 meV from run to run. Mobility and doping values were consistent run to run, within one order of magnitude.

More than 100 tandem CQD solar cells were made in developing the fabrication process, with the best device demonstrating an efficiency of 4.2%. In the course of these studies, we fabricated more than 20 devices with efficiencies greater than 3%.

Grading of stoichiometry, and thus band-edge position, is a concept widely used to great effect in semiconductor quantum electronics, including ultrahigh-frequency heterojunction bipolar transistors[24] and graded-index separate-confinement-heterostructure lasers with low lasing thresholds[25]. The present work provides a benefit to work-function grading and confirms the attractiveness of grading strategies in soft materials such as organic small molecules, polymers and CQDs. The GRL concept can be used to build photovoltaic devices with three or more junctions. Such many-junction devices provide a route to overcoming the charge carrier transport limitations in CQD films today, and, more broadly, they offer the potential to reach well above the Shockley–Quiesser limit.

Table 2 | Electrical properties of the GRL constituent materials.

	E_f (eV)	E_v (eV)	E_c (eV)	n_0 (cm^{-3})
MoO_3	5.4	8.5	5.4	$\sim 10^{19}$
ITO	4.8			
AZO	4.1	7.4	4.1	$\sim 5 \times 10^{19}$
TiO_2	4.1	7.7	4.0	$\sim 5 \times 10^{16}$

E_f, work function; E_v, ionization energy; E_c, electron affinity; n_0, electron free-carrier density.

Methods

Tandem colloidal quantum dot solar cell fabrication. In fabricating the bottom electrode, 10–30 nm TiO_2 nanoparticles, originally dispersed in terpineol (DSL90-T, Dyesol), were further diluted in terpineol and spin-coated onto ITO (Delta Technology) substrates. The nanoparticles were diluted with terpineol (1:3 by weight), spin-cast at 1,500 r.p.m., and placed on a hotplate pre-heated to 120 °C. The substrates were heated at 200 °C for 15 min and 400 °C for 60 min, then underwent $TiCl_4$ treatment in a 60 mM solution in deionized (DI) water at 70 °C for 30 min. The substrates were removed, rinsed with DI water, and heated at 400 °C for 60 min. Bottom electrode processing was carried out in a fume hood in ambient conditions.

For CQD deposition, PbS CQDs (1.6 eV) at a concentration of 25 mg ml^{-1} in octane were deposited in a layer-by-layer fashion. Two drops of CQDs were dispensed onto the substrates through a 0.2 μm filter and spin-cast at 2,500 r.p.m. for 10 s; five drops of a 0.2% mercaptopropionic acid (MPA) in methanol solution were applied to the CQD film through a 0.2 μm filter for 3 s then spin-cast at 2,500 r.p.m. Finally, three rinse steps were carried out, first with methanol, then with acetone, and finally with octane, each followed by spinning the substrate at 2,500 r.p.m. for 10 s. This procedure was repeated until the desired film thickness (~200 nm) was reached (12 layers). The device was post-soaked in 10% MPA in methanol for 30 min, and then rinsed with methanol, acetone and octane. PbS CQDs (1 eV) at 37.5 mg ml^{-1} in octane were deposited on the substrates using the same method to achieve a 300-nm-thick film (10 layers). A 10–30% MPA/methanol solution was used for the solid-state treatment, and no post-soaking step was carried out.

For GRL deposition, MoO_3 (Alfa Aesar) was deposited by thermal evaporation at a rate of 0.4 Å s^{-1}. ITO, AZO and TiO_2 (all from Kurt J. Lesker) were deposited by an RC magnetron sputtering (Angstrom Engineering Åmod deposition) system in a glovebox (Innovative Technology) at room temperature. The 50 nm ITO was sputtered in 1% O_2/Ar environment at a pressure of 5 mtorr and a rate of 0.25 Å s^{-1}, the 50 nm AZO in 1% O_2/Ar at 5 mtorr at a rate of 0.25 Å s^{-1}, and the 40 nm TiO_2 under Ar at 5 mtorr at a rate of 0.20 Å s^{-1}. A thermometer monitoring substrate temperature indicated a rise to no greater than 30 °C.

Tandem CQD solar cell characterization. Tandem CQD solar cells were measured in an inert N_2 environment. The current–voltage characteristics of the tandem CQD solar cells were recorded using a source meter (Keithley). AM1.5 illumination was accomplished using a solar simulator (Science Tech). The illumination area was

apertured to 0.049 cm^2 using two collimated apertures, one in the optical pathway and the other immediately before light impinging on the device under test. The tandem CQD solar cell had a GRL area of 0.18 cm^2 and a top contact area of 0.06 cm^2. An absolute current of 0.5 mA corresponds to ~10 mA cm^{-2} when an illumination area of 0.049 cm^2 is used to calculate the current density.

The EQE spectrum was acquired under AM1.5 white light bias (1 sun bias achieved using a solar simulator) by passing the output of a 400 W Xe lamp through a monochromator and using appropriate filters. The collimated output of the monochromator was measured using calibrated Newport 818-UV and 818-IR power meters. The measurement step was 20 nm. Photocurrent was measured using a lock-in amplifier.

GRL characterization. As detailed in Supplementary Section SI6, UPS was used to obtain the Fermi energies and valence band edges of MoO_3, AZO and TiO_2. X-ray photoelectron spectroscopy (XPS) was used to ascertain elemental composition and chemical state of the constituents of MoO_3, AZO and TiO_2. Cyclic voltammetry was used to obtain the electron affinity of AZO and TiO_2.

References

1. Konstantatos, G. *et al*. Ultrasensitive solution-cast quantum dot photodetectors. *Nature* **442,** 180–183 (2006).
2. Konstantatos, G., Clifford, J., Levina, L. & Sargent, E. H. Sensitive solution-processed visible-wavelength photodetectors. *Nature Photon.* **1,** 531–534 (2007).
3. Clifford, J. P. *et al*. Fast, sensitive and spectrally tuneable colloidal-quantum-dot photodetectors. *Nature Nanotech.* **4,** 40–44 (2009).
4. Rauch, T. *et al*. Near-infrared imaging with quantum-dot-sensitized organic photodiodes. *Nature Photon.* **3,** 332–336 (2009).
5. Sukhovatkin, V., Hinds, S., Brzozowski, L. & Sargent, E. H. Colloidal quantum-dot photodetectors exploiting multiexciton generation. *Science* **324,** 1542–1544 (2009).
6. Sargent, E. H. Infrared photovoltaics made by solution processing. *Nature Photon.* **3,** 325–331 (2009).
7. Gur, I., Fromer, N. A., Geier, M. L. & Alivisatos, A. P. Air-stable all-inorganic nanocrystal solar cells processed from solution. *Science* **31,** 462–465 (2005).
8. Kamat, P. V. Quantum dot solar cells semiconductor nanocrystals as light harvesters. *J. Phys. Chem. C* **112,** 18737–18753 (2008).
9. Luther, J. M. *et al*. Schottky solar cells based on colloidal nanocrystal films. *Nano Lett.* **8,** 3488–3492 (2008).
10. Arango, A. C., Oertel, D. C., Xu, Y., Bawendi, M. G. & Bulovic, V. Heterojunction photovoltaics using printed Colloidal Quantum Dots as a photosensitive layer. *Nano Lett.* **9,** 860–863 (2009).
11. Koleilat, G. I. *et al*. Efficient, stable infrared photovoltaics based on solution-cast colloidal quantum dots. *ACS Nano* **2,** 833–840 (2008).
12. Choi, J. J. *et al*. PbSe nanocrystal excitonic solar cells. *Nano Lett.* **9,** 3749–3755 (2009).
13. McDonald, S. A. *et al*. Solution-processed PbS quantum dot infrared photodetectors and photovoltaics. *Nature Mater.* **4,** 138–142 (2005).
14. Pattantyus-Abraham, A. G. *et al*. Depleted-heterojunction colloidal quantum dot solar cells. *ACS Nano* **4,** 3374–3380 (2010).
15. Lamorte, M. F. & Abbott, D. H. Analysis of AlGaAs–GaInAs cascade solar cell under AM0–AM5 spectra. *Solid-State Electron.* **22,** 467–473 (1979).
16. Lemorte, M. F. & Abbott, D. H. Computer modeling of a two-junction, monolithic cascade solar cell. *IEEE Trans. Electron. Dev.* **27,** 831–840 (1980).
17. Yamaguchi, M., Takamoto, T., Araki, K. & Ekins-Daukes, N. Multi-junction III–V solar cells: current status and future potential. *Solar Energy* **79,** 78–85 (2005).
18. King, R. R. *et al*. 40% efficient metamorphic GaInP/GaInAs/Ge multijunction solar cell. *Appl. Phys. Lett.* **90,** 183516 (2007).
19. Hiramoto, M., Suezaki, M. & Yokoyama, M. Effect of thin gold interstitial-layer on the photovoltaic properties of tandem organic solar cell. *Chem. Lett.* **19,** 327–330 (1990).
20. Yakimov, A. & Forrest, S. R. High photovoltage multiple-heterojunction organic solar cells incorporating interfacial metallic nanoclusters. *Appl. Phys. Lett.* **80,** 1667–1669 (2002).
21. Kim, J. Y. *et al*. Efficient tandem polymer solar cells fabricated by all-solution processing. *Science* **317,** 222–225 (2007).
22. Sista, S. *et al*. Highly efficient tandem polymer photovoltaic cells. *Adv. Mater.* **22,** 380–383 (2010).
23. Kroger, M. *et al*. Role of the deep-lying electronic states of MoO_3 in the enhancement of hole-injection in organic thin films. *Appl. Phys. Lett.* **95,** 012301 (2009).
24. Kurishima, K., Nakajima, H., Yamahata, S., Kobayashi, T. & Matsuoka, Y. Effects of a compositionally-graded $In_xGa_{1-x}As$ base in abrupt-emitter InP/InGaAs heterojunction biopolar transistors. *Jpn J. Appl. Phys.* **34,** 1221–1227 (1995).
25. Chinn, S. R., Zory, P. S. & Reisinger, A. R. A model for GRIN-SCH-SQW diode lasers. *IEEE J. Quantum Electron.* **24,** 2191–2214 (1998).

Author contributions

X.W. and G.I.K. performed all device fabrication and characterization. L.L. assisted in CQD preparation. J.T., H.L., I.J.K., R.D., L.B., D.A.R.B. and S.H. assisted in GRL characterization and data analysis. X.W., G.I.K. and E.H.S. designed the experiments, interpreted the results and wrote the manuscript.

Additional information

The authors declare no competing financial interests. Supplementary information accompanies this paper at www.nature.com/naturephotonics. Reprints and permission information is available online at http://www.nature.com/reprints/. Correspondence and requests for materials should be addressed to E.H.S.